International Journal of Innovative
Computing, Information and Control
Volume **13**, Number **2**, April **2017**

ICIC International ©2017 ISSN 1349-4198
pp. 575–589

OPTIMIZATION OF LIGHT SOURCE POSITION IN APPEARANCE INSPECTION SYSTEM FOR SPECULAR REFLECTION SURFACE

Zhong Zhang[1], Hironobu Yoshioka[1], Shiqing Ren[2]
Takuma Akiduki[1] and Tetsuo Miyake[1]

[1]Department of Mechanical Engineering
Toyohashi University of Technology
1-1 Hibarigaoka Tenpaku-cho, Toyohashi 441-8580, Japan
{ zhang; akiduki; miyake }@is.me.tut.ac.jp

[2]School of Information Science and Engineering
Shenyang Ligong University
No. 6, Nanping Central Road, Hunnan New District, Shenyang 110159, P. R. China
renshiqingcn@126.com

Received August 2016; revised December 2016

Abstract. *Demand for automatic appearance inspection systems for metallic plating parts with specular reflection has been increasing. However, inspection automation is difficult because of reflections from surroundings or because the strong specular characteristics of the specular reflections increase white noise and cause the brightness to saturate. In recent research, we have proposed an algorithm which can eliminate strong specular reflection by using an image processing technique and multiple images with different light sources, and confirmed its effectiveness. In this paper, in order to achieve automatic appearance inspection, we construct a correspondence between the parts of a three-dimensional shape to the conventional plane parts to be inspected, and examine the optimization method of light source positions by using a three-dimensional reflection model. Experiments confirm that optimized light source positions can be obtained by the proposed simulation method.*

Keywords: Appearance inspection, Defect detection, Specular reflection, Reflection model, Light source position, Automatic inspection system

1. **Introduction.** Highly specular reflective surfaces, such as machined surfaces, painted surfaces and plated surfaces are highly reflective, so their inspection is a difficult problem met frequently within the automatic quality control of industrial parts. Because on highly specular reflective surfaces, specular reflection is very strong and diffuse reflections are too weak. Hereafter, we shall call these surfaces highly specular reflective (HSR) surfaces. The visual inspection of the appearance of metal components in most manufacturing processes mainly depends on human inspectors whose performance is generally subjective, variable, and therefore inadequate. A vision inspection system offers objectivity, better reliability and repeatability and is able to carry out defect measurement to evaluate industrial part quality.

To date, a lot of new research results have been reported about vision inspection systems, which has attracted a noteable amount of attention. A typical kind of vision system has been built to inspect defects on HSR surfaces by analyzing the deformation of lighted stripes [1, 2]. Because of the rather heavy formalism involved in computing defect geometry from the deformation of the lighted stripes, these methods, although accurate, are extremely time-consuming. Other typical systems have been proposed which use a novel lighting solution to obtain a signal specular-reduced image and reveal defects. For

(a) 3D Cover-knob (b) 2D chrome-plated parts

FIGURE 1. Examples of chrome-plated parts that are HSR curve surfaces

instance, Gnanaprakasam et al. [3] constructed a lighting system that used a variable intensity white light source, conducted through a fiber optic bundle and focused using a collimator to minimize the divergence angle. Ken et al. [4] designed a lighting system with a programmable array of high-power light-emitting diodes that allows the angle of incident light to be varied over a series of images. The lighting systems proposed are effective at solving the highly specular reflection problem. However, they are incapable of curved surface inspection because specular reflections from the curved surface, which cannot always be avoided in one image, may mask the true location of the objects and lead to incorrect measurements. This is because the curved surface topography is complex and defect properties such as shape, direction and location are complex and varied. Figure 1 shows two photos of chrome-plated parts, which were taken in a natural environment, and exemplifies the above-mentioned appearance and challenge. The environment surrounding the object can be observed because the HSR surfaces of mirror-like objects reflect light rays directly. Some specular reflections completely cover some surfaces, so we do not know whether there are defects in these bright regions. As a result, not all defects on a surface can be illuminated and form recognizable illuminated spots in a single obtained image of an HSR curved surface.

In order to overcome this problem, the techniques use structured lighting systems to turn a set of specular images into a single specular-reduced synthetic image. With regard to these structured lighting systems, Seulin et al. [5, 6] proposed a dynamic lighting system, in which the lighting system is dynamic while the object is static, and is composed of juxtaposed luminous and dark strips. It enables a large number of light transitions to scan the surface and defects are always revealed in dark areas surrounded by luminous ones: it enables the entire defect surface to be revealed. Aluze et al. [7] presented a lighting system that is composed of a planar back light source in front of which a metallic grid is moved at a specific rate. Morel et al. [8] designed an active lighting system, which is a diffuse dome light composed of a ring with numerous LEDs and a dome whose surface is diffuse. In order to provide a uniform and unpolarized light onto the object, the ring of LEDs is split into four parts that can be independently electrically controlled. By using the lighting systems shown above, a set of specular images can be obtained, and simple image processing techniques are then used to segment the synthetic image into defective and non-defective regions. These techniques are quite successful at identifying defects that change the surface normal, but not the surface reflectivity. However, the techniques have an assignment that make the lighting system larger and more complicated, and the light source needs to be controlled according to the objects.

To address the problems above, authors [9, 10] developed a simple lighting system, where only four smaller diffuse illuminates are composed of a variety of illuminate angles.

The lighting system is very simple and is also easy to control. Some experiments on HSR curved surfaces such as chrome-plated acrylonitrile butadiene styrene (hereafter referred to as chrome-plated ABS) resin were carried out using our system. The experiments showed that this system could reliably detect defects on HSR curved surfaces and that the system was robust to the shape and location of the defect which was extracted in the synthetic image reconstructed from a set of images. However, setting the optimal position parameters of the light source is very important for this system. This is because the system needs to capture several images illuminated under different light source directions, and to reconstruct a synthetic image, in which all defects are integrated with high contrast and bright regions are eliminated.

In this paper, in order to set the optimal position parameters of the lighting system, a simulation platform using three-dimensional reflection models is first constructed and an optimization method of light source positions by using the constructed simulation platform is proposed. Finally, the simulation results obtained by the constructed simulation platform are confirmed by the experiments and encouraging results are shown. The remainder of the paper is organized as follows. In the next section, our vision inspection system is introduced and the lighting system is reviewed. A numerical simulation platform for the optimization of lighting system using a rendering method and reflection models is presented in Section 3. Furthermore, in Section 4, the methods of determining the parameters of the reflection models are proposed. And then, in Section 5, some simulation results with HSR curved surfaces for optimization of the light source are demonstrated and good performance of our technique is obtained. Finally, in Section 6, we state the conclusions of this paper.

2. Review of the Vision Inspection System and Lighting System.

Here, the basic structure of visual inspection system and the principle of defect inspection are first introduced, and then the lighting system and its characteristics are described.

2.1. Vision inspection system.

A schematic of the vision inspection system prototype and lighting system are presented in Figures 2 and 3 [9]. As is shown in the figures, the vision inspection system consists of a CCD camera, a lighting system with four light sources and a test table for installing the inspection target. The light source and camera are installed facing the center of the table, with the center-to-center distance between the table and the light source being 330 [mm] and the center-to-center distance between the table and the camera being 550 [mm].

For the camera, we chose the most popular sensor, namely a charge coupled device. It is popular among industrial users mainly because of its high reliability, shock resistance, high sensitivity, resistance to electromagnetic interference and the linearity of its response with respect to luminance. A CCD camera which provides an 8-bit gray scale image was mounted in a fixed position perpendicularly above the work piece.

2.2. Measuring environment and defect inspection procedure.

In our application, the vision inspection system is in a dark room. The object is fixed properly on the work piece. Under certain illumination conditions, the location of the object mainly depends on its surface shape. In the current research, we placed the object to ensure less specular reflections and distinct specular reflective regions from different images. As shown in Figure 2, the defect inspection procedure is performed as follows. First, in the image acquisition stage, four (or more) images are generally captured from the object illuminated by four different incidence directions in turn. Second, the specular processing procedure is performed to remove the specular reflections and enhance defect expressibility. After this processing, all defects are successfully gathered in a synthetic image reconstructed

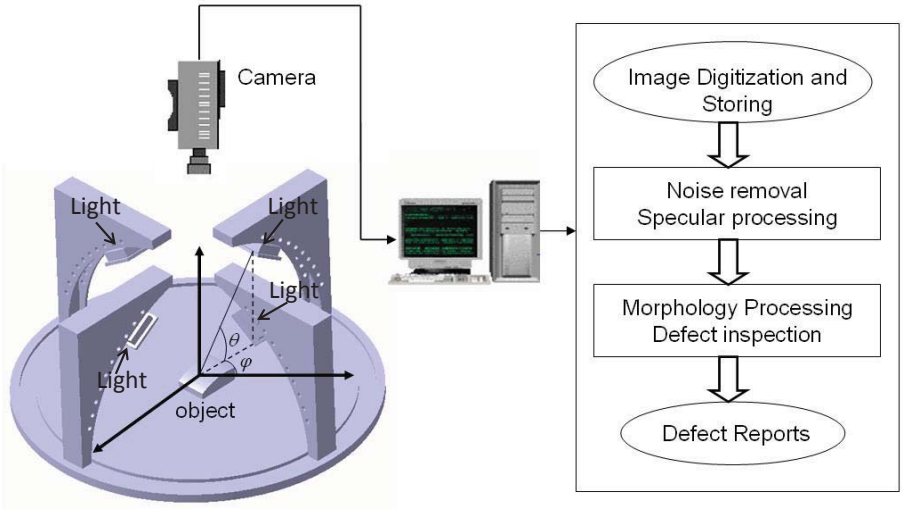

FIGURE 2. The schematic representation of the vision inspection system [9]

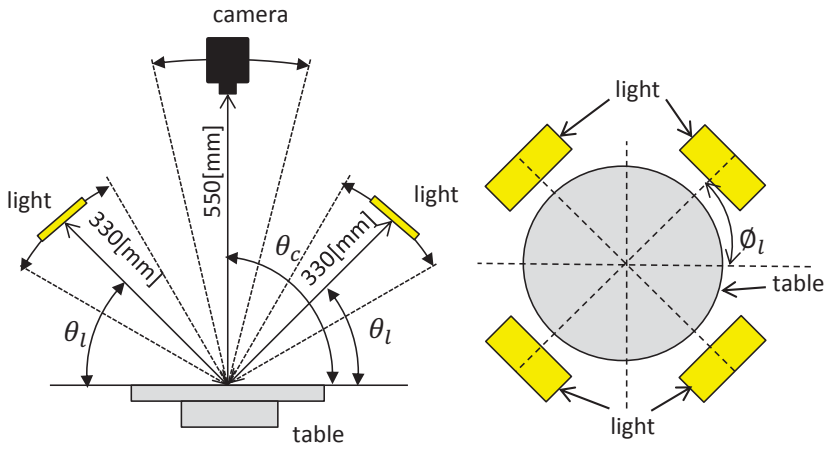

FIGURE 3. Operative space of the light sources and camera

from the input images by using a multi-image reconstruction method [10]. Next, the synthetic image is submitted to the noise-removal stage and all defects are extracted by combining template matching and morphology techniques [11]. Finally, the system outputs the detection results and provides information on whether there are any defects on the surface and other analyses [9].

2.3. **Lighting system.** The choice of a suitable light source is crucial to ensure a reliable analysis of the HSR surface. Different objects require different lighting conditions, and different light sources will affect measurement results. A diffuse light source, which provides intense uniform light in every direction, can eliminate shadows and greatly reduce the effect of specular reflections [12]. The objects in this paper feature very strong specular reflection with weak diffuse reflection [13]. Hence, a diffuse directional light source, that is, a side light source, has been adopted. The light source position is defined by (θ_l, ϕ_l), as shown in Figure 3, where θ_l denotes the vertical angle and ϕ_l denotes the horizontal angle. This can reduce specular reflection from the surface and enhance edge brightness. This is favorable for inspecting objects with highly specular or uneven surfaces. In this vision inspection system, a square LED with white light and a separate constant current source with an intensity control were adopted. Many experiments with HSR curved surfaces,

such as chrome-plated surfaces, show that the defects to be detected are clearer compared with the surrounding region under proper light intensity and incidence direction. However, specular reflection from HSR curved surfaces cannot be completely avoided through the use of a uniform diffuse light source. On the other hand, a variety of defects which have different geometric shapes and locations may not be illuminated or covered by bright regions. That is, the surface defects cannot be obtained correctly and completely from a single image of an HSR surface. So, as shown in Figure 3, the lighting system has been specially designed in the proposed vision inspection system. A group of light sources are mounted on their own rack. The light source distribution and illumination parameters play an important role in obtaining favorable images. They mainly depend on the topography and optical properties of the object under investigation.

3. **A Numerical Simulation Platform for Optimization of Lighting System.** Numerical simulation is a flexible, practical tool for efficiently investigating vision inspection system hardware and software design for myriad industrial applications. Simulated images can aid in both image understanding and vision inspection system design, significantly reducing the engineering time required to design and successfully implement a vision inspection system. In this section, we will create a numerical simulation platform to optimize the lighting system by using a rendering method and reflection models.

3.1. **Rendering method.** For performing numerical simulation on a computer, rendering methods currently studied in the field of computer graphics are effective. Rendering methods can be divided into two kinds, one of which is a local rendering method that considers only the irradiation of the direct light from the light source, and the other is a global rendering method which considers the inter-reflections from the object and the surrounding walls as well as the irradiation of light from the light source. In this study, the images measured by our vision inspection system have been captured in a black box, in which reflections off the inner walls in the box are suppressed, so all reflectional light is cut out except for the inspection light source and reflection from the outside onto the target object surface. Therefore, the local rendering method is used in this study.

The reflection characteristic is defined as the properties of reflection strength and reflection direction when the light emitted from the light source radiates the object surface, and it will vary substantially depending on the material and the smoothness of the object surface. This reflection characteristic is expressed by a bi-directional reflectance distribution function (BRDF) [14]. The BRDF at a point on the object surface depends on the bi-direction of the reflection and incidence, and is defined as the ratio of the intensity of the incident light from the illumination direction and the intensity of the reflected light to the viewing direction. The reflection model is intended to embody the BRDF to enable its use in such applications as actual computer graphics (CG) and computer vision (CV). In our research, the reflection models are applied to the local rendering method and the simulation platform of the lighting system is used.

3.2. **Reflection models.** Reflection off metallic surfaces is different from that off inhomogeneous surfaces. In the case of the inhomogeneous (dielectric) material, the following four reflected light elements have been considered: 1) specular reflection that reflects once off a surface which is flatter than the wavelength of the incident light; 2) diffuse reflection that has reflected two or more times off a rough surface, which consists of material smaller in size than the wavelength of the incident light; 3) diffuse reflection that is diffracted on the surface, which consists of material not greater in size than the wavelength of the incident light. Usually, the reflected light element can almost be disregarded because it is very small except when the surface of the object has a periodic structure of order roughly

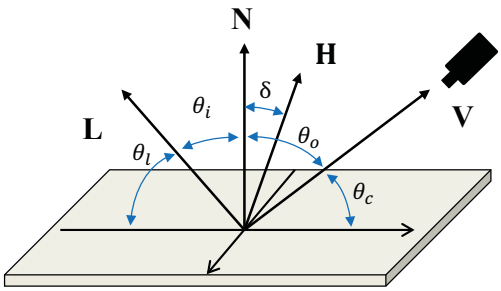

FIGURE 4. The vectors related to reflection in the reflection models

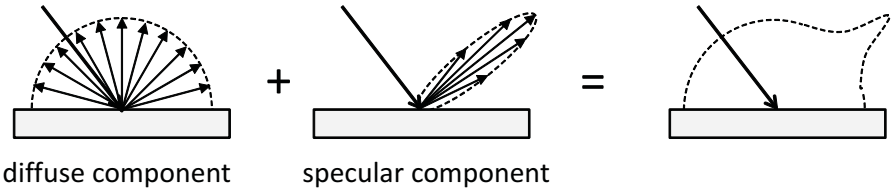

FIGURE 5. Schematics of the diffuse and specular components

equivalent to the wavelength of the light; 4) diffuse reflection that first penetrated the surface, and then escaped the surface after a repetition of reflections with colored matter (pigment) on the inside of the dielectric material.

In the case of reflected light off a metallic material there is no fourth element. This is because the metallic material has conductive electrons, so the electric field of the light is covered by Dolude's Law and the light cannot enter the metal. Furthermore, refection off a metallic surface is different from that off a dielectric surface. For one thing, the reflections have different polarization properties. For unpolarized incident light, the reflected light off a metallic surface is still unpolarized, while the reflected light off an inhomogeneous surface is polarized. A second reason is that for smooth metallic surfaces, specular reflection is very strong and diffuse reflection is too weak. Moreover, the surroundings are often observed as specular reflections. In this study, therefore, we consider only two reflection components, namely the specular reflection of the first reflection element and diffuse reflection of the second reflection element, because the ABS surface is a metallic chrome-plated surface.

Figure 4 shows the vectors related to reflection in the reflection models, where the direction of vector **L** denotes the illumination direction, the direction of vector **V** denotes the viewing direction, and the direction of vector **N** denotes normal direction at point x of the surface. Here, it is assumed that vector **H** bisects the angle between vector **V** and vector **L**. In addition, θ_i is the angle between vector **N** and vector **L**, θ_o is the angle between vector **N** and vector **V**, δ is the angle between vector **N** and vector **H**.

The reflection components reflected from the object surface in this study, as shown in Figure 5, are approximated as a sum of the specular reflection component I_s and the diffuse reflection component I_d. Therefore, the reflected light intensity of the object surface I can be expressed as the following expression.

$$I = I_d + I_s \tag{1}$$

3.2.1. *Diffuse reflective characteristics and reflection model.* As is shown in Figure 5, the diffuse reflection components are assumed to be the reflected components generated by the incident light which are diffusely reflected at the surface two or more times. The

reflected light, therefore, is scattered uniformly, and is observed at uniform intensity from all directions.

For a diffuse reflection model, there is the Lambert model, which assumes the intensity of diffuse reflection is proportional to the cosine of the angle between the normal direction and the direction of the light source, and is widely used. The following Equation (2) shows Lambert's model.

$$I_d = R_d \max(0, \mathbf{N} \bullet \mathbf{L}) \tag{2}$$

where I_d represents the intensity of the diffuse reflection component and R_d diffuse reflectance coefficient. When the angle between the normal direction $\mathbf{N}$ and the direction of the light source $\mathbf{L}$ exceeds 90 [deg], the surface becomes light non-irradiation and shadow, so that the cosine takes a negative value. In this case, I_d is replaced with zero by the function max.

3.2.2. *Specular reflective characteristics and reflection model.* The specular reflection component has a property in which it reflects once off a surface, which is flatter than the wavelength of the incident light. When the object surface is completely smooth, specular reflection is ideally observed only in the specular direction. In practice, however, since the minute irregularities exist on the surface of the object, specular reflection, as is shown in Figure 5, has a narrow distribution of specular direction. Therefore, accurate modeling of specular reflection is difficult, and various models corresponding to different purposes have been proposed. Representative specular reflection models include the Phong model [15] and the Torrance-Sparrow model [16]. Compared to the Phong model which is obtained based on experience, the Torrance-Sparrow model is a model that faithfully reproduces the reflection characteristics of the object surface based on physical analysis. The main differences of these models appear when the incident angle θ_i is large. In this case, the Torrance-Sparrow model has much stronger specular reflection, and the peak occurs at a larger angle than the specular reflection angle. This phenomenon is called off-specular and is measured in real environments. The Torrance-Sparrow model can be shown as the following Equation (3):

$$I_s = \frac{R_s}{\cos\theta_o} \exp\left(-\frac{\delta^2}{2\sigma^2}\right) \tag{3}$$

where parameter R_s is the specular reflection coefficient and represents the specular reflectivity of the surface, and is such that a higher value corresponds to a stronger reflection. Parameter σ represents the concentration of the specular reflection component in the specular direction, and the specular reflection component is observed sharply and strongly as the σ value is smaller. In expression (3), the off-specular can be reproduced when the angle θ_o of incident light is larger, because parameter R_s is multiplied by $\frac{1}{\cos\theta_o}$. In this study, our purpose is to reproduce the surface reflection characteristics of the actual object. Therefore, the Torrance-Sparrow model is selected.

3.3. **Geometry of the measurement object.** In order to estimate the surface normal vector $\mathbf{N}$, we need to know the object's surface shape. Here, the geometric shape of the object can be obtained from three-dimensional CAD data of vector data that is created during the design of the object. Figure 6(a) shows an example of the vector data of the object shown in Figure 1(a). In order to apply the information of this geometry in the calculation of the reflection model, the three-dimensional (3D) CAD data needs to be converted into the Stereo Lithography (STL) file format, which approximately represents the 3D shape surface by a set of small triangle patches. On the smooth surface, it is possible that the brightness often changes rapidly by specular reflection, although there are a few instances in which the brightness changes rapidly due to diffusion reflection.

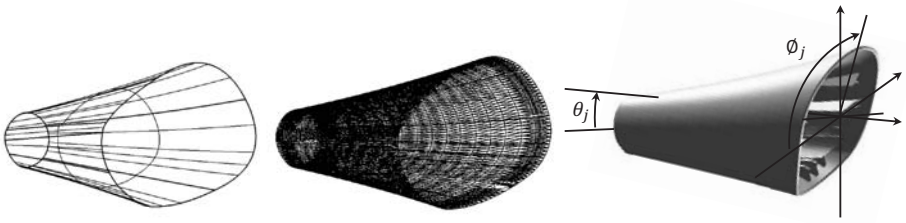

FIGURE 6. 3D CAD model of the object surface

In this study, because it is necessary to faithfully depict the change in luminance due to specular reflection, it is necessary to set the size of the triangular patches. Here, in order to faithfully depict rapid changes in brightness due to specular reflection, we set the size of the triangular patches to be smaller than the camera resolution required for surface inspection. Figure 6(b) shows the shape data of the object with the created STL format. In addition, the object surface obtained by CG using STL format is shown in Figure 6(c) and the object's posture can be shown by (θ_j, ϕ_j) using the elevation angle θ_j and the rotating angle ϕ_j.

4. **Estimating Coefficients of the Reflection Models.** In order to achieve the numerical simulation platform for representing the reflection characteristics of an object surface by the reflection models using the rendering method, it is necessary to set parameters such as the reflection coefficients to match the object surface. Therefore, in this section, the methods of estimating the reflection parameters of the object surface are introduced, when virtualizing the test environment based on the real environment. For the reflection models as described in Section 3.2, the Lambert model is used to render the diffuse reflection component, and the Torrance-Sparrow model is used to render the specular reflection component.

4.1. **Surface light source model.** While a point light source irradiates the surface from a single direction, a surface light source irradiates the same portion of the surface from multiple directions. Therefore, the surface light source has the characteristic where it becomes easy to illuminate defects on the object surface. Based on this reason, the present study adopts the LED surface light source. However, the diffuse reflection model and specular reflection model shown in Section 3.2 model the reflection of light irradiated from a certain point, so they are able to be applied only with a point light source. Here, to simplify the problem, we assume that a surface light source is a set of multiple point light sources, and propose the surface light source model shown in Figure 7. The number of the point light sources in the surface light source is one in Figure 7(a), four in 7(b), nine in 7(c) and sixteen in 7(d). Here, the light source shown in Figure 7(a) can be also regarded as the point light source. When the number of the point light source is m, the brightness value on the surface to be illuminated by the surface light source can be calculated by the following Formula (4).

$$I = \sum_{k=1}^{m} (I_{d,k} + I_{s,k}) \tag{4}$$

where the number m is the point light source number in a surface light source.

4.2. **Estimating method of diffuse reflection model coefficient.** In order to estimate the diffuse reflection coefficient R_d, two types of images are used, one of which is the measured image with only the diffuse reflection component on the object surface and

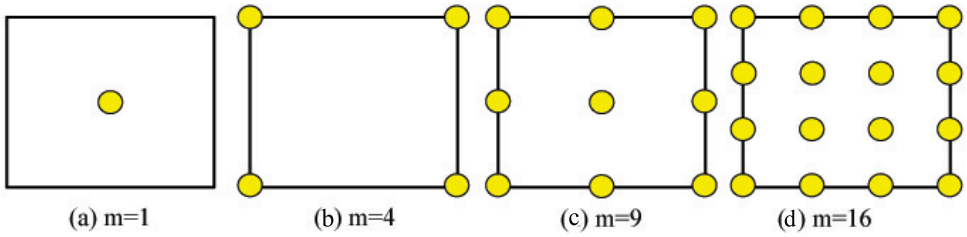

FIGURE 7. Variation of surface light source by the point light sources, where m shows number of the point light sources

the other is the simulated images created by the method shown in Section 3.3 using the CAD data. Next, the light source direction vector $\mathbf{L}$, the normal vector $\mathbf{N}$ of the object surface and the initial value of diffuse reflection coefficient R_d are substituted into the Lambert model in Equation (2), and the diffuse reflection components are estimated and a simulation image having the reflection components is created. Then, the ratio E_d and the difference value D between the average brightness value B_d of the measured image and the average brightness value B_r of the estimated image with the diffuse reflection components are calculated.

$$E_d = \frac{B_r}{B_d} \tag{5}$$

$$D = |B_r - B_d| \tag{6}$$

By comparing the different value D with the threshold λ_d, if the difference D is larger than the threshold λ_d, then we update the diffusion reflection coefficient R_d by following Equation (7) and the processing returns to the beginning.

$$R_d = E_d R_d \tag{7}$$

On the other hand, if the difference D is smaller than threshold λ_d, then the current diffuse reflection coefficient R_d is considered as the estimated value and the process is ended.

4.3. **Estimating method of specular reflection model coefficients.** In the same way as estimating the diffusion reflection coefficient, in order to estimate the specular reflection coefficient, two types of images are used, one of which is the measured image with the specular reflection component on the object surface and the other is the simulated images created by the method shown in Section 3.3 using the CAD data. The estimation procedure can be shown as follows.

(1) First, the initial values of the specular reflection coefficient R_s and the parameter σ of the object surface in Equation (3) are set. It has been reported by Ward [17] that the parameter σ of the object in the real environment is in the range of 0.001-0.2. Therefore, in this experiment, the initial value of the parameter σ was set to 0.01. The specular reflection coefficient R_s was set to the luminance saturation value 255 of the specular reflection region in the measured image.

(2) Then, the view angle θ_o of the camera, the initial values of the specular reflection coefficient R_s and the parameter σ, the surface normal vector $\mathbf{N}$ and the angle δ of the vector $\mathbf{H}$ are substituted into the Torrance-Sparrow model shown in Formula (3), and the specular reflection components are calculated. Furthermore, the simulated image with the specular reflection component is created.

(3) To determine the size of the specular reflection area of the simulation images, the pixels having N_s levels of brightness saturation due to the specular reflection in the simulation images are counted, and the difference S_1 between N_s and N_m that is the

pixel number of brightness saturation due to specular reflection of the measured image is calculated. Furthermore, the ratio E_s between N_s and N_m is also calculated, by the following equations.

$$S_1 = |N_m - N_s| \tag{8}$$

$$E_s = \frac{N_m}{N_s} \tag{9}$$

At this time, if the difference S_1 is larger than the threshold λ_{s1}, then it is assumed that the sizes of the specular reflection area between these two images are different, and we update the specular reflection coefficient R_s and returns the process to step (2) by the following conditions.

$$R_s = E_s R_s \tag{10}$$

On the other hand, if the difference S_1 is smaller than the threshold λ_{s1}, then we proceed to the threshold determination for the spread of the specular reflection.

(4) For the strength of the specular reflection in the simulation image, the difference S_2 between the total brightness value of the specular reflection components of the simulation image and that of the measured image is calculated, and if S_2 is less than the threshold λ_{s2}, then the σ is changed by the σ_{step} and the process is returned to step (1). On the other hand, if S_2 is larger than the threshold value λ_{s2}, then it is considered that the characteristics of the specular reflection area in the simulation image is the closest to that of the measured image, and R_s and σ of this time are referred to as the estimated value.

4.4. **Experiment results and discussion.** Figure 8 shows an example of the images measured by using the experimental device shown in Figures 2 and 3, where Figure 8(a) shows the image measured in the condition of light source position when $(\theta_l, \phi_l) = (60°, 45°)$, and Figure 8(b) shows the image measured in the condition of light source position when $(\theta_l, \phi_l) = (60°, 135°)$, where the object posture is $(\theta_j, \phi_j) = (0°, 0°)$. In the case of Figure 8(a), the measured image does not have any specular reflection component. Opposite to this, in the case of Figure 8(b), the measured image has some specular reflection components. Therefore, the image shown in Figure 8(a) will be used to estimate the diffuse reflection coefficient R_d and the image shown in Figure 8(b) will be used to estimate the specular reflection coefficient R_s and parameter σ.

Table 1 shows the estimated reflection coefficients by following the method shown in Sections 4.2 and 4.3 and Figure 9 shows the created simulation image by using these coefficients. In our experiment, the number m of point light sources that make up the surface light source is different, for example, Figure 9(a) is a case where $m = 1$, Figure 9(b) is a case where $m = 4$, Figure 9(c) is a case where $m = 9$, and Figure 9(d) is a case where $m = 16$. In Table 1, the value of the diffuse reflection coefficient R_d does not depend on the number m of the point light sources and it was constant. In contrast, the specular reflection coefficient R_s and parameter σ depend on the number m of the point light sources. Here, we extract only the luminance saturation region by specular reflection from the simulation image, and compare the area and perimeter of the area with that of the measured image. The result is that the light source conditions in the case of $m = 4$ are able to reproduce the specular reflection area more accurately. The same result can be obtained by using the other measured images. That is, the surface light source model proposed is effective for the creation of the simulation images, and the number $m = 4$ of the point light sources in the surface light source is valid. Therefore, in this study, the diffusion reflection coefficient, the specular reflection coefficient and the parameter σ,

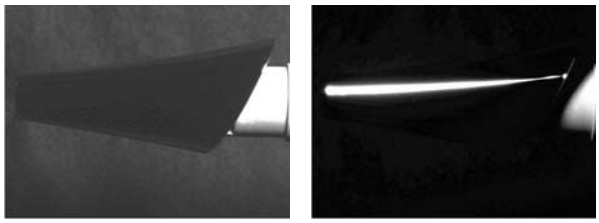

(a) $(\theta_l, \emptyset_l) = (60^o, 45^o)$ (b) $(\theta_l, \emptyset_l) = (60^o, 135^o)$

FIGURE 8. Example of lighting object image measured, where the object posture is $(\theta_j, \phi_j) = (0°, 0°)$

TABLE 1. Estimated results of specular and diffuse reflection coefficients in the condition of the surface light sources with different number m of the point light sources

	m	R_d	R_s	σ
(a)	1	45.0	1180000	0.0525
(b)	4	45.0	12500	0.0475
(c)	9	45.0	16200	0.045
(d)	16	45.0	23000	0.0425

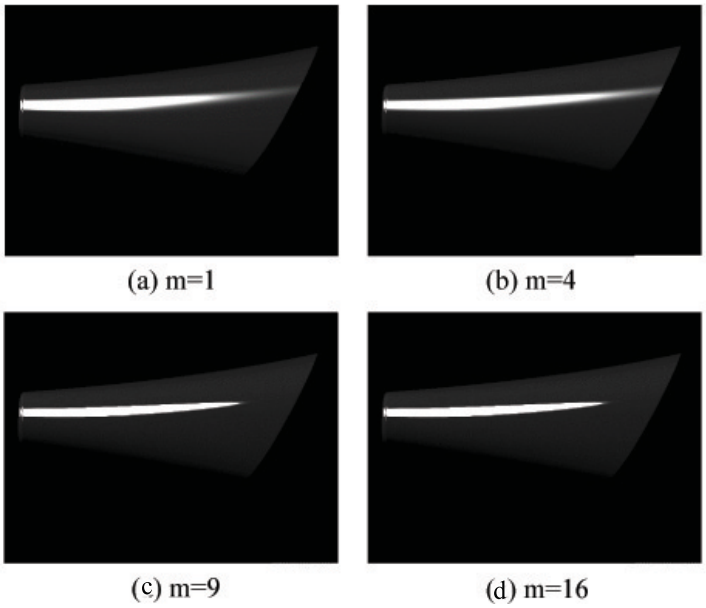

FIGURE 9. Simulated images, which are in the object posture $(\theta_j, \phi_j) = (0°, 0°)$ and constructed by using estimated reflection coefficients

which are obtained in the condition of surface light source with $m = 4$, will be used to create the simulation platform and carry out the optimization of the light source position.

5. **Optimization of Inspection Light Source Position.** In this section, in order to optimize the position of the inspection light source, the reflection simulation of the object surface is carried out by using the constructed simulation platform in the condition of changing the position of the light source and the posture of the object.

5.1. **Optimizing condition.** Because the optimum conditions of the light source position need to be determined based on the specular reflection removal process, here the

procedure of specular reflection removal process is first described. The specular reflection removal process is achieved by reconstructing a new synthetic image from a set of images, which are captured under a fixed viewpoint and different light source directions [10]. The procedure is as follows. First, a set of images is captured from different light source directions. Second, the intensity gradient of each input image taken with a certain light source direction is calculated. The information of the luminance gradient is retained in the case where a large luminance gradient of the adjacent pixels is present in the same position for the other images. In contrast, the information of the luminance gradient is removed in the case where it is not present in the same position for the other images. Then a new gradient image from all input images is obtained to eliminate outliers. Finally, a synthetic image is reconstructed from the new gradient data. The synthetic image will be used for further processing, for example, defect inspection.

As can be seen from the above steps, one image, in which the specular reflection area is removed and the information of defect is held, can be created by satisfying the following conditions: 1) the position of the specular reflection region does not overlap those of the other images; 2) the reflection by the same defect can be confirmed by two or more images. Furthermore, since the reconstructed synthetic image is used for defect detection by template matching, it is required to extract the feature information from the image which contains defects with high signal noise ratios. Therefore, the condition of creating a synthetic image in which the specular reflection component is removed and the stable feature information of the defects is extracted, is determined as the optimization conditions of the light source positions.

5.2. **Optimization procedure.** The procedure of the optimization technique is as follows.

(1) Perform surface reflection simulation by using the constructed simulation platform for the object under all the conditions of surface light source positions and create the reflected luminance data group.
(2) Select a combination of four surface light sources positions (angles) from the number of surface light source position conditions and create a luminance matrix from the reflection luminance data group. The column elements of the luminance matrix are set as the angle condition of the surface light source position, and the row elements are set as the number of the surface polygons.
(3) Descend by column of the brightness matrix, and create a new evaluation matrix by removing the rows of the first and fourth. In this way, it becomes possible to remove the surface light source position conditions which have many shaded regions having a lower brightness and many specular reflection regions having a high brightness.
(4) Each element value for the evaluation matrix with two rows is evaluated by using the threshold value and is reset to zero when it is determined to be in a shaded area or a specular reflection area.
(5) Calculate the sum of all element values for the evaluation matrix and set the sum value as the evaluation value of the surface light source combination.
(6) Calculate the evaluation values of all the surface light source combinations and set a condition of the highest evaluation value as the optimal combination condition of the surface light source position (angle).

5.3. **Optimization results and discussion.** In this section, the reflection simulation of the object surface is carried out by following the optimization procedure shown above and the optimization of the surface light source position is performed. The simulation conditions are set according to the experimental apparatus shown in Figures 2 and 3

TABLE 2. Results of the optimization for light source position (θ_l, ϕ_l) in the condition of different object posture (θ_j, ϕ_j), where the object posture was adjusted by changing the rotation angle ϕ_j, but the elevation angle is fixed at $\theta_j = 0$ [deg]

			Light1		Light2		Light3		Light4	
		θ_c	θ_l	ϕ_l	θ_l	ϕ_l	θ_l	ϕ_l	θ_l	ϕ_l
$\phi_j =$	0	105	60	45	60	135	60	225	60	315
	82	105	60	45	60	135	60	225	60	315
	180	105	60	45	60	135	60	225	60	315
	278	105	60	45	60	135	60	225	60	315

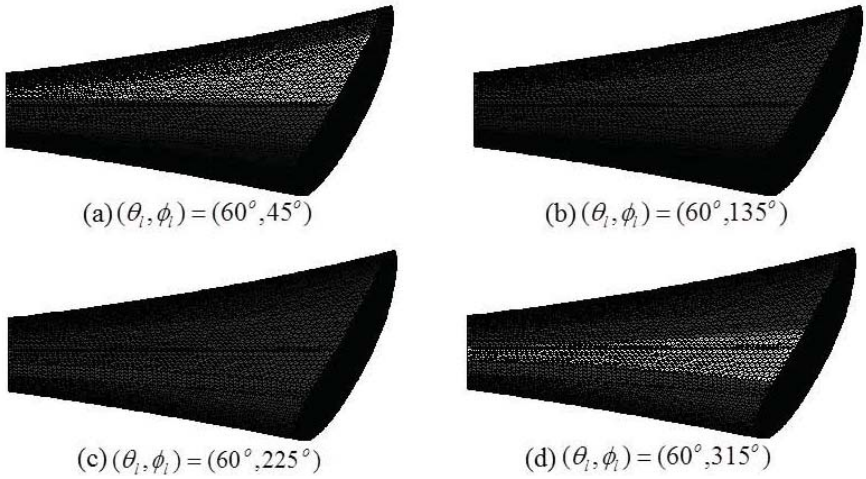

FIGURE 10. Example of the surface reflection simulation images, where the object posture is $(\theta_j, \phi_j) = (0°, 278°)$

and, the position of the surface light source is represented by the horizontal angle ϕ_l and the vertical angle θ_l. In the experimental apparatus, since the horizontal angle ϕ_l of the surface light source is fixed at the four angles $\phi_l = 45, 135, 225, 315$ [deg], it is possible to adjust the position of the surface light source by the vertical angle θ_l in the range 30-60 [deg].

The example of the target object is a Cover-knob shown in Figures 1(a) and 6. It can be seen from Figure 6 that the surface consists of four curved surfaces approximately, and the posture is adjusted by changing the elevation angle θ_j and the rotating angle ϕ_j. It was confirmed by simulation that inspection of the entire surface of the object is possible by fixing $\theta_j = 0$ [deg] and rotating $\phi_j = 0, 82, 180, 278$ [deg], when setting the basic posture to $(\theta_j, \phi_j) = (0°, 0°)$. That is, the four images, which are measured in the condition of the postures $(\theta_j, \phi_j) = (0°, 0°)$, $(0°, 82°)$, $(0°, 180°)$ and $(0°, 278°)$, can be over all the surface of the object. In this time, therefore, optimization is only carried out with these four postures by changing the light source positions.

The optimization results obtained by using the constructed simulation platform are shown in Table 2, and the examples of the surface reflection simulation images are shown in Figure 10, which is obtained under the optimized surface light source condition of the posture $(\theta_j, \phi_j) = (0°, 278°)$. As shown in Figure 10, there is no overlapping area of specular reflection area in the case of different light source directions, so it is possible to satisfy the optimization conditions of the light source. In addition, confirmation experiments have been carried out and an example is shown in Figure 11, where Figure (I) shows the

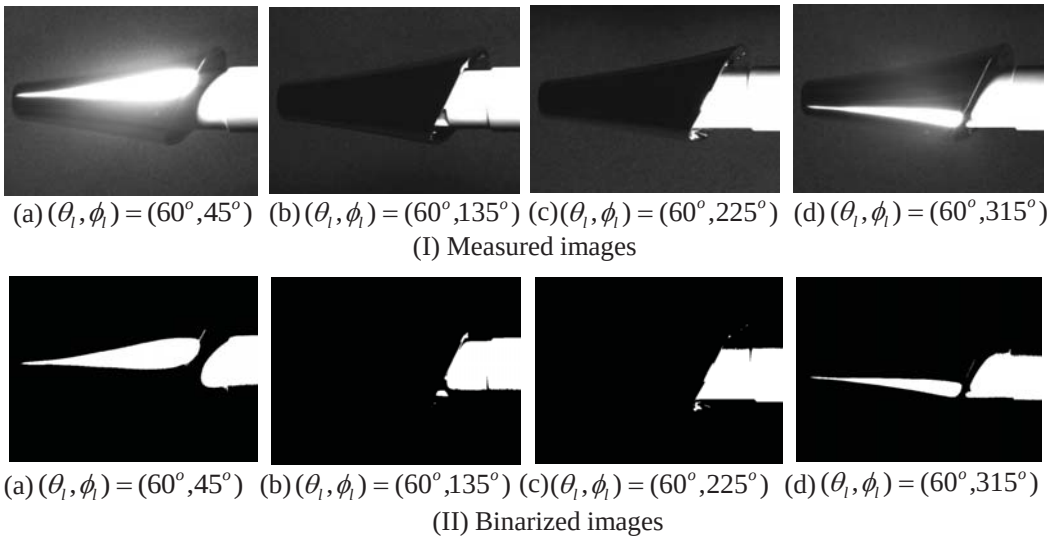

FIGURE 11. Measured and binarized images by using our vision inspection system, where the object posture is $(\theta_j, \phi_j) = (0°, 278°)$

measured images and (II) shows the binarized images. And for both Figures (I) and (II), (a) has the condition $(\theta_l, \phi_l) = (60°, 45°)$, (b) has the condition $(\theta_l, \phi_l) = (60°, 135°)$, (c) has the condition $(\theta_l, \phi_l) = (60°, 225°)$ and (d) has the condition $(\theta_l, \phi_l) = (60°, 315°)$. And the object posture is $(\theta_j, \phi_j) = (0°, 278°)$. It can be seen from Figure 11 that the specular area almost occurred in different positions and these areas do not overlap each other. And the same result can also be obtained in the other conditions shown in Table 2. Therefore, it can be said that the proposed optimization method was effective for optimization of the light source positions, because optimization of lighting conditions was able to be met in all four postures. By this optimization method using the simulation platform configured, it is considered that the purpose of automatically and optimally setting the light source positions for each object can be achieved, not the conventional manual setting.

6. **Conclusions.** In this paper, in order to set the optimal illumination parameters of a lighting system, we first created the simulation platform by a rendering method using three-dimensional reflection models and then proposed an optimization method of light source positions. The main results obtained can be shown as follows.

1) The numerical simulation platform was constructed by the rendering method using the reflection models and it was a useful tool for the optimization of the lighting system.
2) The surface light source model and the estimating method of coefficients of the reflection models have been proposed and their effectiveness has been confirmed.
3) The optimization method of the lighting system using a numerical simulation platform was proposed in this research and some simulation results with HSR curved surfaces showed good performance.
4) Finally, confirmation experiments of the optimization method were carried out and encouraging results were obtained.

However, in this paper, the ease of defect detection has not yet considered in the condition of the light source optimization. In future, the ease of the defect detection will be considered in the condition of the light source optimization, and practical use of the proposed method will be aimed for.

REFERENCES

[1] S. K. Nayar, A. C. Sanderson, L. E. Weiss and D. A. Simon, Specular surface inspection using structured highlight and Gaussian images, *IEEE Trans. Robotics and Automation*, vol.6, no.2, pp.208-218, 1990.

[2] S. Ajalingappaa and B. Ramamoorthy, Defect detection and classification of zinc coated parts using machine vision, *Proc. of the 11th International Symposium on Measurement and Quality Control*, pp.1-4, 2013.

[3] P. Gnanaprakasam, J. M. Parker, S. Ganapathiraman and Z. Hou, Efficient 3D characterization of raised topological defects in smooth specular coatings, *Image and Vision Computing*, vol.27, pp.319-330, 2009.

[4] S. Ken, M. B. Gary and C. David, Defect identification on specular machined surfaces, *Machine Vision and Applications*, vol.25, pp.377-388, 2014.

[5] R. Seulin, F. Merienne and P. Gorria, Dynamic lighting system for specular surface inspection, *Proc. of SPIE Machine Vision Applications in Industrial Inspection IX*, vol.4301, pp.199-206, 2001.

[6] R. Seulin, F. Merienne and P. Gorria, Simulation of specular surface imaging based on computer graphics: Application on a vision inspection system, *EURASIP Journal on Applied Signal Processing*, vol.7, pp.649-658, 2002.

[7] D. Aluze, F. Merienne, C. Dumont and P. Gorria, Vision system for defect imaging, detection, and characterization on a specular surface of a 3D object, *Image and Vision Computing*, vol.20, pp.569-580, 2002.

[8] O. Morel, C. Stolz, F. Meriaudeau and P. Gorria, Active lighting applied to three-dimensional reconstruction of specular metallic surfaces by polarization imaging, *Applied. Optics.*, vol.45, no.17, pp.4062-4068, 2006.

[9] C. J. Li, Z. Zhang, I. Nakamura, T. Imamura, T. Miyaki and H. Fujiwara, Developing a new automatic vision defect inspection system for curved surfaces with highly specular reflection, *International Journal of Innovative Computing, Information and Control*, vol.8, no.7(B), pp.5121-5136, 2012.

[10] C. J. Li, Z. Zhang, T. Miyake, T. Imamura and H. Fujiwara, Processing specular reflection components of chrome-plated surface by multi-image reconstruction method, *International Journal of Computer Information Systems and Industrial Management Applications*, vol.1, pp.303-311, 2009.

[11] Z. Zhang, I. Nakamura, C. J. Li, T. Imamura, T. Miyake and H. Fujiwara, Metal plating surface defect detection by template matching using morphological processing, *ICIC Express Letters, Part B: Applications*, vol.2, no.3, pp.615-620, 2011.

[12] R. Seulin, F. Merienne and P. Gorria, Simulation of specular surface imaging based on computer graphics: Application on a vision, inspection system, *EURASIP Journal on Applied Signal Processing*, vol.2002, no.7, pp.649-658, 2002.

[13] Z. Zhang, S. Ren, T. Miyaki, H. Fujiwara and T. Imamura, Processing reflections on metallic surfaces using a special random sampling method, *International Journal of Innovative Computing, Information and Control*, vol.4, no.7, pp.1595-1606, 2008.

[14] A. Ngan, F. Durand and W. Matusik, Experimental analysis of BRDF models, *Eurographics Symposium on Rendering*, 2005.

[15] B. T. Phong, Illumination for computer-generated images, *Proc. of Special Interest Group on Computer GRAPHics (SIGGRAPH'75)*, pp.311-317, 1975.

[16] K. E. Torrance and E. M. Sparrow, Theory for off-specular reflection from roughened surfaces, *Proc. of Journal of the Optical Society of America*, vol.57, no.9, pp.1105-1112, 1967.

[17] G. J. Ward, Measuring and modeling anisotropic reflection, *Proc. of Special Interest Group on Computer GRAPHics (SIGGRAPH'92)*, vol.26, pp.256-272, 1992.